International Journal of Fluid Mechanics & Thermal Sciences
2026, Vol. 12, No. 1, pp. 16–23
https://doi.org/10.11648/j.ijfmts.20261201.12

Research Article

Modeling of Ventilation Characteristics Formed by Jet in Cross Flow

Ju-Song Pak, Myong-Jin Jo, Kwang-Il Ri*

Faculty of Naval Architecture and Ocean Engineering, Kim Chaek University of Technology, Pyongyang, DPR Korea

Abstract

It is important to accurately model and analyze the ventilation characteristics formed by jet in cross flow (JICF) of liquid around a plate. Through 3D numerical simulations (using FLUENT), design of experiment (DOE) and regression, a mathematical model is constructed to accurately describe the process of formation of ventilated cavity by gas jet in cross flow of the liquid phase. Multiphase flow and turbulence models are established to reflect the formation and development of the ventilated cavity, and a reasonable simulation plan is established by means of design of experiment, and a regression model is obtained through nonlinear regression. A reasonable simulation plan is established to model the different factors impact on the size of the ventilation cavity and to comprehensively reflect its effect. Ventilation characteristics formed by JICF are then compared with experimental results. The results of various comparative analyses show that the 3D simulation method presented in this paper can more accurately reflect the ventilated cavity formation and, with this, evaluate the ventilation characteristics and make the design reasonably with the mathematical model obtained through design of experiment nonlinear regression. It is of great significance in many applications, including pump jet propeller design, by optimizing the design to meet the given design conditions with reasonable variations of parameters.

Keywords

JICF, Ventilation Characteristics, Design of Experiment, Numerical Simulation

1. Introduction

The jet in cross flow (JICF) is widely used in natural phenomena and industrial applications. Examples are gas cooling of turbine blades [1, 2], fuel atomization in aero-engines [3], thrust vector control in rocket engines [4, 5], and blade boundary layer flow control. The jet is gradually bent by the action of the cross-flow, and exhibits complex hydrodynamic phenomena such as separation, reattachment, and swirl flow through the cross-flow and energy and momentum exchange.

KAMOTANI et al. [6] were the first authors to describe the jet orifice downstream flow field structure. The presence of a pair of counter rotating vortex (CVP) in the cross-section downstream of the jet orifice can be observed, where the downstream flow field is dominant and its influence range is up to the far downstream region of the jet orifice. As the experimental techniques and numerical simulation methods have been developed continuously, people have begun to study the causes of the formation of various complex vortex structures during the development of cross-jet flows.

*Correspondence: Kwang-Il Ri (GI.Li803@star-co.net.kp)

Received: 6 October 2025; **Accepted:** 8 November 2025; **Published:** 25 February 2026

KOZLOV et al. [7] suggested that the cause of shear layer vortices is K-H instability caused by the velocity difference between jet and transverse flow, which is further attributed to quasi-periodic fluctuations and breakdown of the interface. At the same time, many scholars have found that strong three-dimensional and unsteady properties exist in the transverse jet flow field and that the jet-initiated flow field vortex structure can generate complex interactions with each other during the evolution process [8, 9].

Over the past 70 years, people have already been more aware of the turbulent structure evolution of transverse jet flow, but this work has largely focused on gas-gas single-phase transverse jet flow.

Professor CECCIO at the University of Michigan [10, 11] developed a good study of gas jet flow in liquid-phase cross-flow based on gas-layer resistance reduction, and the correlation experiments established the gas-phase structure in a flat plate model through air-entrainment mode, and the results indicate that three different states can be formed, such as decreasing bubble resistance, decreasing air-layer resistance and decreasing the transient resistance between the two.

Due to the complexity of the research question, we have not yet formed a system's understanding of how the gas jet flow in liquid cross-flow affects the behavior and the change rules of bubbles in different stages of the development of the flow field, for macroscopic description [12, 13], which focuses heavily on the evolution of bubble shape evolution of gas jet formation.

Recently, with the advent of engineering applications, some scholars have conducted preliminary studies on the relationship between vortex structure and bubble evolution in the gas jet flow field in liquid cross-flow.

Wang Yung [14] performed numerical simulations of flat plate ventilation using different models to capture the horseshoe vortex near the jet orifice and the counter-rotating vortex pair inside the jet gas, and found that the vortex structure has a distinct feature at different stages of gas stratification.

ZHENG et al. [15] developed numerical calculations for the aeration assimilation of a rotating body, and the results indicate that the instability of the aerated cavitation liquid interface and the evolution of the vortex structure are closely related.

Based on the numerical results, MAG H et al. [16, 17] analyzed the evolution mechanism of underwater vehicle surface gas jet, captured the counter-rotating vortex pair inside the gas jet, and suggested that the pure gas phase region of the initial stage of the gas jet mainly dominates the counter-rotating vortex pair. Compared to gas-gas single-phase transverse jet flow, the gas jet flow field structure in liquid-phase transverse flow is a typical multiphase flow field, and the significant difference in the physical properties of the gas-liquid two-phase medium can generate the vortex structure change process in the single-phase transverse jet flow, which can further change the momentum exchange and transfer mechanism between the jet gas and the main fluid.

To further investigate the evolution of the gas jet flow field structure in liquid-phase cross-flow, we performed numerical simulations of the underwater gas cross-jet multiphase flow based on the two-stage projection method and the VOF interface trapping method, and analyzed in detail the evolution of the vortex structure in the two-phase cross-jet field.

As seen from the above previous analysis, there have been many studies on the mechanism of the formation of the aeration cavity by gas jets in a horizontal flow of fluid around a plate, but no studies have been reported to accurately and quantitatively evaluate the process.

2. Numerical Simulation and Mathematical Modeling

2.1. Numerical Calculation Method

2.1.1. Solver Setting

(i). Multi-phase Model

As the multi-phase model, the Mixture model is used. The Mixture model is used for more than two fluid simulations that can be mixed together and considers the relative velocity between phases. Typically, it can be used to model phenomena such as non-Newtonian fluids, bubble flow, and deposition. [18, 19]

The governing equations of the Mixture model are:

Continuity equation:

$$\frac{\partial}{\partial t}(\rho_m)+\nabla\cdot\left(\rho_m\vec{v}_m\right)=0 \tag{1}$$

Momentum equation:

$$\frac{\partial}{\partial t}\left(\rho_m\vec{v}_m\right)+\nabla\cdot\left(\rho_m\vec{v}_m\vec{v}_m\right)=-\nabla p+\nabla\cdot\left[\mu_m\left(\nabla\vec{v}_m+\nabla\vec{v}_m^T\right)\right] \tag{2}$$

Transport equation:

$$\frac{\partial}{\partial t}(\alpha_v\rho_v)+\nabla\cdot\left(\alpha_v\rho_v\vec{v}_m\right)=R_e-R_c \tag{3}$$

where

ρ_m —density of mixture

v_m —velocity of mixture

α_v —volume fraction of vapor

ρ_v —density of vapor

R_e, R_c —evaporating and cooling rate of vapor

(ii). Turbulence Model

The most commonly used turbulence models include the *k*-

ω model and the k-ε model. The ω-equation has several advantages over the ε-equation. The most typical is that the equation can be integrated without additional terms in the viscous sublayer. Hence, the k-ω model is also called the y^+ insensitive model. Moreover, the k-ω model is more accurate in simulating boundary layer flow. In general, the k-ω model is not used in the simulation of low Reynolds number flows. The k-ω model includes standard k-ω, BSL(Baseline) k-ω, and SST (Shear Stress Transport) k-ω models. The standard k-ω model is an empirical model based on the model transport equation for turbulent kinetic energy (k) and specific dissipation rate (ω), which can also be considered as the ratio of ω to k.

Transport equation:

$$\frac{\partial}{\partial t}(\rho k)+\frac{\partial}{\partial x_i}(\rho k u_i)=\frac{\partial}{\partial x_j}(\Gamma_k \frac{\partial k}{\partial x_j})+G_k \quad (4)$$

$$\frac{\partial}{\partial t}(\rho \omega)+\frac{\partial}{\partial x_i}(\rho \omega u_i)=\frac{\partial}{\partial x_j}(\Gamma_\omega \frac{\partial \omega}{\partial x_j})+G_\omega \quad (5)$$

In these equations, G_k is the generation term of turbulent kinetic energy due to the mean velocity gradient, and G_ω is the generation term of ω.

2.1.2. Boundary Condition of Model

Figure 1 shows the calculation region and boundary condition for simulation.

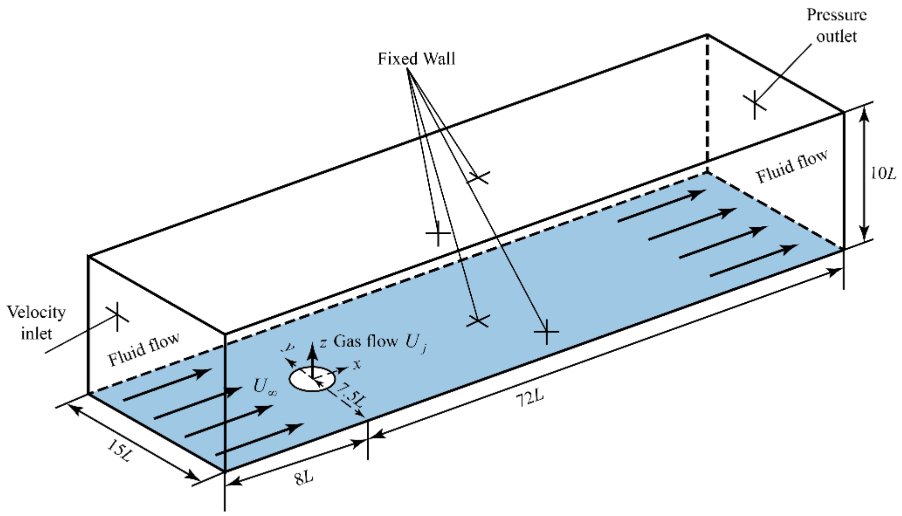

Figure 1. *Computational domain and boundary conditions.*

The computational domain is 80L long, 15L wide and 10L high. The boundary conditions are set as the velocity inlet on the left side and pressure outlet on the right side and the fixed wall on the remaining sides. The circular vent is located at the bottom of the computational domain as the gas velocity inlet. The center of the vent is 8L from the velocity inlet, 7.5L from the side wall, and the diameter is d=0.5L [20]. The material is chosen as the main material and its characteristics are as follows:

$$\rho_{Liquid}=997\text{kg}/\text{m}^3,\ \mu_{Liquid}=8.9011\times10^{-4}\text{pa}\cdot\text{s}$$

Air is chosen as an auxiliary material. The property of air at 25 ℃ is:

$$\rho_{Air}=1.225\text{kg}/\text{m}^3,\ \mu_{Air}=1.7894\times10^{-5}\text{pa}\cdot\text{s}$$

2.1.3. Meshing and Evaluation of Correctness

Since the ventilation cavity is a very complex phenomenon, the influence of mesh on the calculation accuracy is very large. We perform mesh meshing of different sizes and analyze their accuracy based on different mesh accuracy criteria. Since the simulation domain is square, we construct a structured mesh. The constructed mesh is shown in Figure 2.

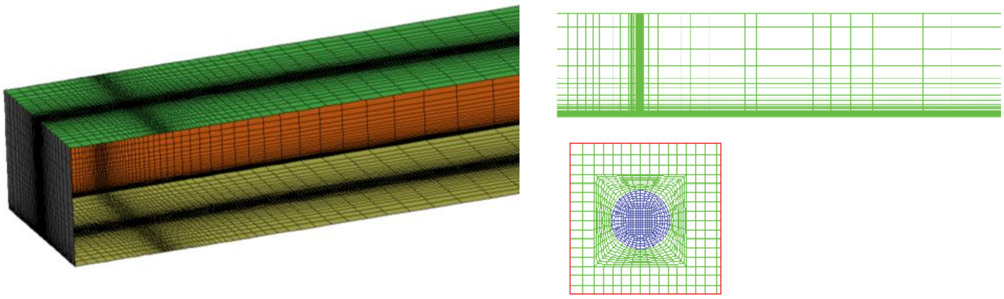

Figure 2. *Mesh of computational domain.*

The minimum degree of mesh distortion is 0.6, which indicates that the mesh is relatively well-meshed. The grid independence test is performed. The test results show that the results converge relatively when the number of meshes is about 900,000. The results of the mesh independence test are shown in Figure 3.

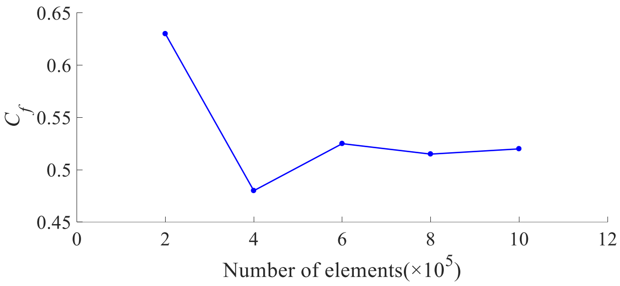

Figure 3. *Force coefficients calculated for different grids.*

2.1.4. Accuracy Verification of Numerical Methods

The proposed mesh is used to verify the accuracy of our simulation method. The accuracy of our simulation method is verified through comparison with experimental data presented in [20, 21]. The simulation is carried out with the inlet flow rate U_∞=0.1 m/s as the same velocity condition as the experimental data and varying the air jet velocity from U_j=0.1 to 0.6 m/s. Figure 1 shows the experimental results and the simulation results. As seen in the figure, the simulation results and experimental results are very similar.

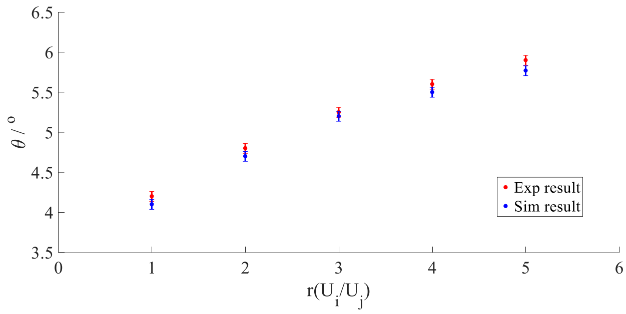

Figure 4. *Comparison of experimental results with simulation results.*

The detailed numerical analysis is shown in Table 1. The expansion angle of the jet at a distance of an integer number of the air jet radius is measured and compared with the experimental data.

Table 1. *Comparison of experimental and simulation results.*

No	1	2	3	4	5
Exp, °	4.23	4.83	5.25	5.64	5.91
Sim, °	4.17	4.72	5.05	5.52	5.77
Absolute error, °	0.060	0.110	0.200	0.120	0.141
Relative error, %	1.41	2.27	3.80	2.12	2.36

The errors between the actual and simulated values are all less than 5%, which indicates that the proposed simulation method is relatively accurate.

2.2. Design of Experiment and Mathematical Model Decision

2.2.1. Design of Experiment and Simulation

As a uniform test design factor, the fluid flow rate U_∞, the gas jet velocity U_j, and the diameter of the jet hole diameter *d* are selected. When the factor number is 3, the centralized-L_2 bias value is analyzed to select the most reasonable uniform test design.

Table 2. *Centralization-L_2 bias of different plans.*

Plan	$U_5(5^3)$	$U_6(6^3)$	$U_7(7^3)$	$U_7^*(7^3)$	$U_8^*(8^3)$	$U_9(9^3)$
CD_2	0.457 0	0.265 6	0.372 1	0.213 2	0.168 1	0.310 2
Plan	$U_9^*(9^3)$	$U_{10}^*(10^3)$	$U_{11}(11^6)$	$U_{11}^*(11^3)$	$U_{12}^*(12^3)$	$U_{13}(13^3)$
CD_2	0.198 0	0.200 0	0.264 9	0.230 7	0.183 8	0.230 8

As can be seen from the table, for the $U_8^*(8^3)$ scheme, the centralization-L_2 bias is the smallest, 0.1681. This scheme is chosen as a uniform test design scheme, and then a range of values for each parameter is determined. A uniform test design is carried out based on the range of values of the defined factors. The results of the uniform test design according to the $U_8^*(8^3)$ scheme are shown in Table 3.

Table 3. *Simulation plans with uniform test design.*

Plan	Cross flow velocity U_∞, m/s	Jet velocity U_j, m/s	Jet hole diameter d, mm
1	0.1	0.25	8
2	0.15	0.45	7
3	0.2	0.2	6
4	0.25	0.4	5
5	0.3	0.15	8.5
6	0.35	0.35	7.5
7	0.4	0.1	6.5
8	0.45	0.3	5.5

The simulation is carried out based on the established uniform test design scheme. The simulation results obtained under different conditions with the above-mentioned simulation method are shown in Figure 5.

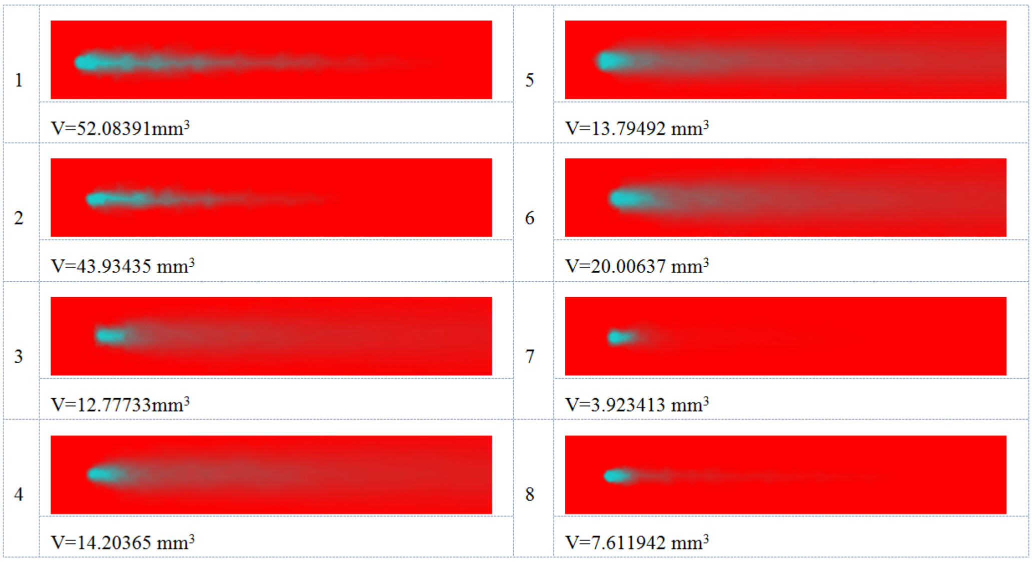

Figure 5. *Volume of cavitation at different plans.*

As shown in the figure, the magnitude of the aeration cavity produced by the variation of the parameters is significantly different. Hence, it is necessary to determine an accurate mathematical model considering the influence of different factors on cavitation formation and to analyze the cavitation characteristics based on the mechanism.

2.2.2. Decision of Mathematical Model

To construct a regression model, the independent variables must be centered and dimensionless first. The regression model uses a quadratic model.

$$y = \beta_0 + \beta_1(U_\infty - 0.275) + \beta_2(U_j - 0.275) + \beta_3(d - 0.275) + \beta_{11}(U_\infty - 0.275)^2 + \beta_{22}(U_j - 0.275)^2 + \beta_{33}(d-5)^2 + \beta_{12}(U_\infty - 0.275)(U_j - 0.275) + \beta_{23}(U_j - 0.275)(d - 0.5) + \beta_{13}(U_\infty - 0.275)(d-5) + \varepsilon$$

Applying the least squares method using the established quadratic model, we obtain the following regression coefficients:

Table 4. Regression coefficients.

No	β_0	β_1	β_2		β_{11}
	14.52	-84.53	54.25	5.83	763.23
No	β_{22}	β_{33}	β_{12}	β_{23}	β_{13}
	β_3 60.85	-3.64	84.63	-39.57	18.32

3. Results

The corresponding table of variance analysis is given in Table 5.

Table 5. Table of variance analysis (SAS result).

Factor	DOF	Error	Variance	F value	P_{rob}>F
Model	3	0.40488	0.13496	595.722	0.0001
Error	3	0.00068	0.00023		
Total error	6	0.40556			
R^2	0.9983				
C.V.	2.79813				

The obtained regression model is substituted by the factors reflected in the simulation scheme to perform a comparison analysis with the simulation results. The simulated results at different test points and the comparison with the regression results are shown in Figure 6.

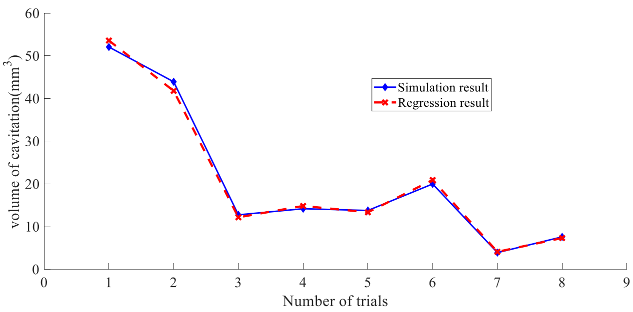

Figure 6. Regression analysis.

4. Discussion

There have been no related results mentioned about the volume of ventilated cavitation created by the JICF. So, in this discussion only the comparison between the simulation and regression results has been done. Table 6 presents the results of detailed numerical and error analysis.

Table 6. Error analysis of simulation results and regression results.

No	1	2	3	4
Sim, mm^3	52.08	43.93	12.77	14.20
Reg, mm^3	53.59	41.80	12.19	14.85
Absolute error, mm^3	1.51	-2.13	-0.58	0.65
Relative error, %	2.89	4.84	4.53	4.57
No	5	6	7	8
Sim, mm^3	13.79	20.00	3.92	7.61
Reg, mm^3	13.37	20.93	4.11	7.34
Absolute error, mm^3	-0.42	0.93	0.19	-0.27
Relative error, %	3.04	4.64	4.84	3.54

The errors between the simulated results and the predicted values by the regression formula are all less than 4%, which indicates that the regression model obtained is relatively accurate. Using this regression model, further research is needed to accurately predict and evaluate the size of the air entrainment formed in the fluid flow.

5. Conclusion

To obtain a regression model for the accurate calculation of the size of the ventilated cavity formed by jet in cross flow (JICF), design of experiment theory and numerical analysis by ANSYS Fluent are used.

First, a 3D numerical simulation method is established to accurately model the generation characteristics of the ventilated cavity. A new simulation method is established to simulate the air-entrainment phenomena in a realistic way by optimizing the multiphase flow model and turbulence model and performing a fine mesh. Through comparative analysis with experimental results presented in the literature, the established simulation method is verified to be relatively accurate.

Second, with the established simulation method, a mathematical model is constructed that accurately captures the ventilation behavior through uniform test design and regression. Regression analysis is performed to verify the accuracy of the established regression model, and this mathematical model can accurately predict and estimate the ventilation behavior in the cross-flow and make a reasonable design.

Further studies on other specific conditions, including the influence of temperature on the development of the air cavity around the plate, can be carried out to perform a comprehensive analysis.

Abbreviations

JICF	Jet in Cross Flow
CVP	Counter Rotating Vortex
DOE	Design of Experiment

Acknowledgments

The authors thank the associate editor and the anonymous reviewers for their insightful comments and valuable suggestions on improving this article.

Funding

This work was partially supported by State Academy of Sciences.

Conflicts of Interest

The authors declare no conflicts of interest.

References

[1] WANG, X. D., KANG, S., Numerical simulation on the slot film cooling field at the leading edge of a turbine cascade., J. Eng. Therm., 2008, vol. 29, pp. 1835-1838.

[2] QIN, Y., REN, J., JIANG H. D., Effects of streamwise pressure gradient on film cooling effectiveness., J. Eng. Therm., 2014, vol. 35, pp. 461-464.

[3] PANDEY, K. M., MEMBER, I., SIVASAKTHIVEL, T., Recent advances in scramjet fuel injection a review. Int. J. Chem. Eng. App., 2010, vol. 14, pp. 294-301.

[4] CHAI, X., IYER, P. S., MAHESH, K., Numerical study of high-speed jets in cross flow. J. Fluid. Mech., 2015, vol. 785, pp. 152-188., https://doi.org/10.1017/jfm.2015.612

[5] CHEN, Z., SHAN, Y., SHEN, X. G., et al., Numerical study on thrust reverser controlled with secondary flow. J. Prop. Tech., 2014, vol. 35, pp. 1181-1187., https://doi.org/10.13675/j.cnki.tjjs.2014.09.005

[6] KAMOTANI, Y., GREBER, I., Experimental investigation of jets in a crossflow., AIAA J., 1972, vol. 10, pp. 1425-1470., https://doi.org/10.2514/3.50386

[7] KOZLOV, V. V., GREK, G. R., LITVINENKO, Y. A., Visualization of conventional and combusting subsonic jet instabilities., Springer. Nature., 2016, pp. 23-34.

[8] SAU, A., SHEU, T. W. H., HWANG, R. R., et al., Three-dimensional simulation of square jets in cross-flow. Phy. Review. E., 2004, vol. 69, pp. 1-20.

[9] LÜ, Y. F., WEI, H. P., LIU, T. T., et al., Numerical investigation of the round jet in crossflow at high velocity ratios with special emphasis on the evolution of vortex structures., Phy. Fluid., 2022, vol. 34, pp. 034-116.

[10] CECCIO, S. L., Fraction drag reduction of external flows with bubble and gas injection. An. Rev. Fluid. Mech., 2000, vol. 42., pp. 183-203., https://doi.org/10.1146/annurev-fluid-120710-101115

[11] ELBING, B. R., WINKEL, E. S., LAY, K. A., et al., Bubble-induced shin-fraction reduction and the abrupt transition to air-layer drag reduction., J. Fluid. Mech., 2008, vol. 612, pp. 201-236., https://doi.org/10.1017/S0022112008003029

[12] BALZAN, M. A., HERNANDEZ, F., LANGE, C. F., et al. Parametric study of the frequency of bubble formation at a single orifice with liquid crossflow., J. Fluids. Eng., 2019, vol. 141, pp. 091-102., https://doi.org/10.1115/1.4042755

[13] DONG, P., WANG, K., CHENG, D., et al., Submerged gas jet in liquid cross flow modeling and flow structures analysis., Ocean. Eng., 2021, vol. 242, pp. 110-128., https://doi.org/10.1016/j.oceaneng.2021.110128

[14] LIU, T. T., WANG, G. Y., ZHANG, N. M., et al., Analysis of vortex dynamics of gas-liquid two-phase crossflows around a porous plate., Act. Arm., 2017, vol. 38, pp. 1375-1384.

[15] WANG, Z. Y., HUANG, B., ZHANG, M. D., et al., Experimental and numerical investigation of ventilated cavitating flow structures with special emphasis on vortex shedding dynamics., Int. J. Mul. Flow., 2018, vol. 98, pp. 79-95.

[16] MA, G. H., CHEN, F., YU, J. Y., et al., Effect of pressure-equalizing film on hydrodynamic characteristics and trajectory stability of underwater vehicle with injection through one or two rows of venting holes. J. Fluid. Eng., 2018, vol. 140, pp. 091-103., https://doi.org/10.1115/1.4039519

[17] MA, G. H., CHEN, F., YU, J. Y., et al., Flow mechanism and characteristics of pressure-equalizing film along the surface of a moving underwater vehicle. J. Fluid. Eng., 2018, vol. 140, pp. 041-103., https://doi.org/10.1115/1.4038394

[18] HUANG, J. K., ZHAO, X., Numerical simulations of atomization and evaporation in liquid jet flows. Int. J. Mu. Flow., 2019, vol. 119.

[19] ROLF, R., On chorine's projection method for the incompressible navier-stokes equations. Lecture Notes in Mathematics, 1992, 1530.

[20] ISMAIL, B. C., URMILA, G., Procedure for estimation and reporting of uncertainty due to discretization in CFD applications., J. Fluid. Eng., 2008, vol. 130, pp. 078001., https://doi.org/10.1115/1.2960953

[21] LÜ, Y, F., ZHANG, M. J., LIU, T. T., et al., Numerical simulation of gas-liquid two-phase flows for two holes ventilated cavities near wall of the flat plate. Dig. Ocean. Und. War., 2021, vol. 4, pp. 279-287., https://doi.org/10.19838/j.issn.2096-5753.2021.04.004